DOI: 10.1002/ejic.200601015

A Square-Planar Nickel(II) Monoradical Complex with a Bis(salicylidene)-diamine Ligand

Laurent Benisvy,[a] Ramu Kannappan,[a] Yu-Fei Song,[a] Sergey Milikisyants,[b] Martina Huber,[b] Ilpo Mutikainen,[c] Urho Turpeinen,[c] Patrick Gamez,[a] Leonardo Bernasconi,[d] Evert Jan Baerends,[d] František Hartl,[e] and Jan Reedijk*[a]

Keywords: Phenoxyl radicals / Nickel(II) complexes / Redox chemistry / Spectroelectrochemistry / EPR spectroscopy / Density functional calculations

The new square-planar Ni^{II}–N_2O_2 complex [Ni(^{Me}L)] (**1**^{Me}), where ^{Me}L stands for the dianionic phenolato form of *N*,*N*′-bis(3,5-di-*tert*-butyl-salicylidene)-4,5-dimethyl-1,2-phenylenediamine ($^{Me}LH_2$), has been synthesised and fully characterised. X-ray crystallography was also used for the characterisation. The electrochemical one-electron oxidation of **1**^{Me} produces the thermally stable (within the temperature range 10–295 K) cationic species (**1**^{Me})$^+$. The UV/Vis and X-band EPR experimental data, supported by DFT calculations, indicate that (**1**^{Me})$^+$ is best described as a Ni^{II} monoradical complex and, thus, does NOT exist in a Ni^{III} ground state, in contrast to its demethylated counterpart [Ni(^{H}L)]$^+$ (**1**^{H})$^+$ below 170 K.

There has been much current interest in the nature and properties of d-transition-metal complexes in which one or more of the ligands are present in a radical state.[1] This interest has been stimulated by the observation and study of so-called "radical enzymes" in nature,[2] as illustrated by galactose oxidase (GO) that uses, in its active form, a phenoxyl radical directly bound to a Cu^{II} centre to perform two-electron oxidation reactions.[3] Further, metal complexes bearing radical-type ligands may exhibit novel physical properties. In some cases, valence tautomerism [M^{n+1}–$^-$OPh] ↔ [M^{n+}–$^{\cdot}$OPh] occurs, which is of relevance for the construction of molecular switches.[4] For these reasons, a thorough understanding of the factors governing the locus of the oxidation (metal versus ligand) is of importance.

Consequently, various suitably protected phenol-containing ligands were designed and successfully applied to stabilise a phenoxyl radical state when coordinated to a transition metal.[1a] With nickel, various Ni^{III} species have been characterised.[5] Recently, De Castro et al. investigated bis(salicylidene)diamine-type ligands at Ni^{II} centres. Oxidation of the complexes in various polar solvents (S_Y) yielded the corresponding octahedral Ni^{III} species [Ni^{III}(L)$(S_Y)_2$]$^+$.[5i–5n] At the same time, two research groups have independently reported that one-electron oxidation of the square-planar complexes [Ni^{II}(^{R}L)] {^{R}L = a dianionic Schiff-base ligand with a cyclohexylene-1,2-diamine backbone (^{Cy}L*)[6] and a phenylene-1,2-diamine (^{H}L) backbone[7]} (see structure below) produces, in dichloromethane, a Ni^{III} complex [Ni^{III}(^{R}L)]$^+$ at sufficiently low temperature and a Ni^{II} radical complex [M^{II}(^{R}L$^{\cdot}$)]$^+$ (^{R}L$^{\cdot}$ = phenoxyl radical anion of ^{R}L) above 190 K. These interesting results have been interpreted in terms of temperature-dependent tautomerism.[6,7]

Herein we report the synthesis and characterisation of the analogous dimethylated complex [Ni(^{Me}L)] (**1**^{Me}) (^{Me}L contains the 4,5-dimethylphenylene-1,2-diamine backbone) and its one-electron oxidised product [Ni(^{Me}L)]$^+$. Surprisingly, experimental EPR spectroscopic and UV/Vis spectroelectrochemical data reveal that the oxidised species does NOT exist in a Ni^{III} ground state in the studied low-temperature range, in contrast to its counterparts [Ni(^{H}L)]$^+$ and [Ni(^{Cy}L)]$^+$.[6,7] Instead, it can be best formulated as a Ni^{II} monoradical complex [Ni^{II}(^{Me}L$^{\cdot}$)]$^+$. DFT calculations support this assignment, pointing to the negligible effect of the methyl groups when the electronic structures of [Ni(^{H}L)]$^+$ and [Ni(^{Me}L)]$^+$ are compared.

[a] Leiden Institute of Chemistry, Gorlaeus Laboratories, Leiden University,
P. O. Box 9502, 2300 RA Leiden, The Netherlands
Fax: +31-715274671
E-mail: reedijk@chem.leidenuniv.nl
[b] Department of Molecular Physics, Huygens Laboratory, Leiden University,
P. O. Box 9504, 2300 RA Leiden, The Netherlands
[c] Department of Chemistry, Laboratory of Inorganic Chemistry, University of Helsinki,
P. O. Box55, A. I. Virtasenaukio 1, 00014 Helsinki, Finland
[d] Theoretische Chemie, Vrije Universiteit Amsterdam,
De Boelelaan 1083, 1081 HV Amsterdam, The Netherlands
[e] Van't Hoff Institute for Molecular Sciences, Homogeneous and Supramolecular Catalysis, Universiteit van Amsterdam,
Nieuwe Achtergracht 166, 1018 WV Amsterdam, The Netherlands

Supporting information for this article is available on the WWW under http://www.eurjic.org or from the author.

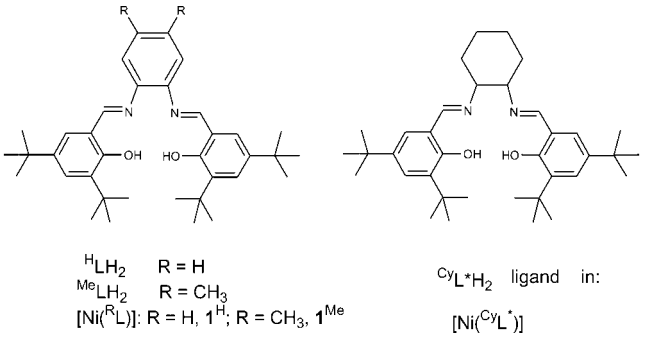

The tetradentate ligand *N*,*N*′-bis(3,5-di-*tert*-butyl-salicylidene)-4,5-dimethylphenylene-1,2-diimine ($^{Me}LH_2$) was synthesised by the condensation of 4,5-dimethylphenylene-1,2-diamine with 3,5-di-*tert*-butyl-salicylaldehyde, as previously reported.[8] The reaction of $^{Me}LH_2$ with $Ni(ClO_4)_2{\cdot}6H_2O$ (1:1) in methanol leads to the formation of red, needlelike crystals of [Ni(^{Me}L)] ($\mathbf{1}^{Me}$) in 77% yield. The molecular structure of $\mathbf{1}^{Me}$ (Figure 1), determined by X-ray crystallography at 173 K, reveals a Ni^{II} centre with a square-planar N_2O_2 coordination sphere defined by the two imine nitrogen atoms [N(30), N(40)] and the two phenolate oxygen atoms [O(10), O(20)] of ^{Me}L. As expected, the structure and molecular dimensions of $\mathbf{1}^{Me}$ are almost identical to those of $\mathbf{1}^{H}$ (see Table S1).[7] Thus, the Ni–O and Ni–N bond lengths [1.853(3)–1.861(2) Å] are short. The mean deviation from the least-squares plane defined by Ni(1), O(10), O(20), N(30) and N(40) is 0.11 Å, with a dihedral angle of 9.6° between the O(10)–Ni(1)–N(30) and O(20)–Ni(1)–N(40) planes.

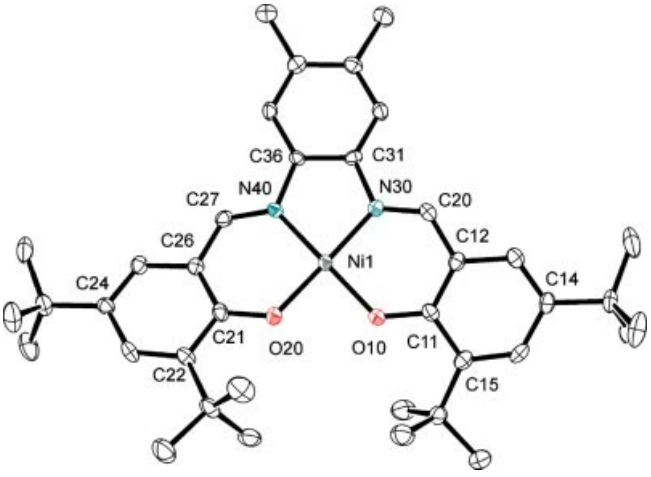

Figure 1. ORTEP representation of [Ni(L^{Me})] ($\mathbf{1}^{Me}$) shown with 50% thermal ellipsoids, as determined at 173 K. The hydrogen atoms are omitted for clarity. Selected bond lengths [Å] and angles [°] for **1**: Ni(1)–O(10), 1.856(2); Ni(1)–O(20), 1.861(2); Ni(1)–N(30), 1.856(3); Ni(1)–N(40), 1.853(3); C(11)–O(10), 1.327(4); C(21)–O(20), 1.327(4); C(27)–N(40), 1.321(4); C(36)–N(40), 1.428(4); C(31)–N(30), 1.421(4); C(17)–N(30), 1.318(4) Å. O(10)–Ni(1)–N(40), 173.03(11); O(10)–Ni(1)–N(30), 94.07(11); N(40)–Ni(1)–N(30), 85.63(12); O(10)–Ni(1)–O(20), 86.86(9); N(40)–Ni(1)–O(20), 94.25(11); N(30)–Ni(1)–O(20), 173.37(11)°.

Complex $\mathbf{1}^{Me}$ exhibits no EPR signal, neither in the solid state nor in CH_2Cl_2 solution, at room temperature or at 77 K. This result indicates that $\mathbf{1}^{Me}$ is diamagnetic ($S = 0$), as expected for a low-spin d^8 square-planar Ni^{II} complex. In $CDCl_3$ solution, $\mathbf{1}^{Me}$ exhibits a well-defined ^{1}H NMR spectrum with resonances between 0 and 10 ppm, which also confirms its diamagnetic nature. Similar to that of complex $\mathbf{1}^{H}$,[7] the UV/Vis spectrum of $\mathbf{1}^{Me}$ in CH_2Cl_2 (Figure 2) displays an absorption band at λ_{max} = 385 nm (ε_{max} = 29800 $M^{-1}cm^{-1}$) due to a $\pi\rightarrow\pi^*$ intraligand transition. Another intense absorption band at 499 nm (ε_{max} = 8900 $M^{-1}cm^{-1}$) and a shoulder at 475 nm (ε = 6700 $M^{-1}cm^{-1}$) are assigned to a phenolate→Ni^{II} charge transfer. A weak shoulder at about 600 nm ($\varepsilon < 200\ M^{-1}cm^{-1}$) may correspond to a largely metal-centred (MC) transition. These spectroscopic observations suggest that the square-planar Ni^{II}–N_2O_2 coordination sphere is retained in CH_2Cl_2 solution.

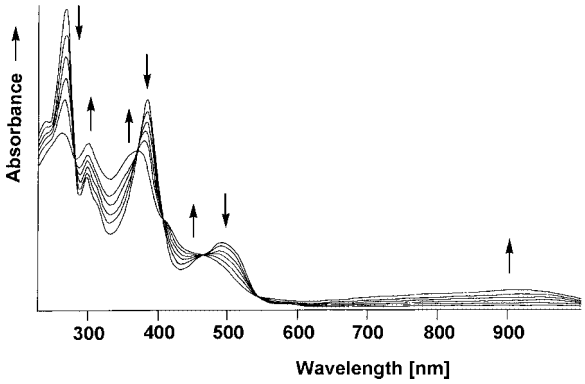

Figure 2. UV/Vis spectroelectrochemistry for the first oxidation of $\mathbf{1}^{Me}$ in CH_2Cl_2 containing $[NBu^n_4][ClO_4]$ (0.3 M) at 293 K.

The cyclic voltammogram (CV) of complex $\mathbf{1}^{Me}$ in dichloromethane (v = 100 mV/s, T = 293 K) exhibits two reversible ($I_{p,c}/I_{p,a}$ = 1) one-electron anodic processes at $E_{1/2}$ = +0.49 V (ΔE_p = 80 mV) and 0.78 V (ΔE_p = 110 mV) vs. Fc/Fc^+ (ΔE_p = 80 mV) used as an internal standard (see Figure S1). These oxidation processes are associated with the formation of $(\mathbf{1}^{Me})^+$ and $(\mathbf{1}^{Me})^{2+}$, respectively. The larger peak-to-peak separation for the second anodic step producing $(\mathbf{1}^{Me})^{2+}$ indicates a slower electron transfer, most likely associated with a change in the molecular structure of the dicationic product. This difference between the anodic steps became more apparent on the longer time scale of the spectroelectrochemical experiments (see below). Interestingly, the $E_{1/2}$ values determined for $\mathbf{1}^{Me}$ are lower than those observed for $\mathbf{1}^{H}$ by 90 and 20 mV for the first and second couple, respectively,[7] and reveal a stabilisation effect of the methyl groups at the phenyl-diene backbone on the oxidised species.

Corresponding UV/Vis spectroelectrochemical experiments with $\mathbf{1}^{Me}$ in the anodic region were performed in dichloromethane at 293 K (Figure 2) and 233 K, with almost identical results. The one-electron-oxidised species

$(\mathbf{1}^{Me})^+$ remains fully stable at both temperatures, as revealed by the completely reversible thin-layer cyclic voltammetric response (with a small ΔE_p value of about 20 mV, which is comparable to that of the Fc/Fc^+ couple) recorded in the course of the anodic and reverse cathodic scans. In the UV/Vis spectral region, the conversion of $\mathbf{1}^{Me}$ to $(\mathbf{1}^{Me})^+$ at room temperature is accompanied by the disappearance of the absorption bands of the parent complex (see Experimental Section) and the growth of new intense bands of the cationic product at λ_{max} (ε_{max}, $M^{-1}\,cm^{-1}$) = 300 (23 200), 374 (22 400), 411 (sh., better resolved at 233 K) and 468 nm(7300); in addition, a broad absorption band of lower intensity appears at a low energy, with poorly resolved maxima at λ_{max} (ε_{max}, $M^{-1}\,cm^{-1}$) = 810 (2100) and 920 nm (2500). The reversibilty of the first anodic step is reflected by the presence of isosbestic points at 280, 375, 405, 466 and 543 nm (Figure 2) and the full recovery of the initial UV/Vis spectrum of $\mathbf{1}^{Me}$ after "back reduction" of $(\mathbf{1}^{Me})^+$. It is important to note that absorption bands at ca. 400 nm (ε_{max} ca. 10 000 $M^{-1}\,cm^{-1}$) are typically found for phenoxyl radical complexes and have been attributed to a $\pi\rightarrow\pi^*$ electronic transition of the phenoxyl ligand.[1a,9] The broad low-energy bands may have their origin in an electron transfer to the phenoxyl singly occupied molecular orbital (SOMO) from lower-lying occupied levels.[10] Thus, one-electron-oxidised $(\mathbf{1}^{Me})^+$ shows the spectroscopic signature of a phenoxyl radical complex, which suggests that the oxidation of $\mathbf{1}^{Me}$ to $(\mathbf{1}^{Me})^+$ is predominantly ligand-centred.

The second anodic step, i.e. the oxidation of $(\mathbf{1}^{Me})^+$ to $(\mathbf{1}^{Me})^{2+}$, is characterised by a large separation between the anodic and reverse cathodic peaks of the couple observed in the thin-layer cyclic voltammogram exceeding 500 mV at 233 K. This result points to a significant difference between the ultimate molecular structures of $(\mathbf{1}^{Me})^+$ and $(\mathbf{1}^{Me})^{2+}$. The electronic absorption spectrum of $(\mathbf{1}^{Me})^{2+}$ (not shown) exhibits a very intense band at 300 nm with a shoulder at 325 nm, two less intense bands of similar intensities at 420 and 455 nm and a weak band at 558 nm. The absorption maximum at 820 nm disappeared and the broad, low-energy absorption band shifted more to the NIR region relative to $(\mathbf{1}^{Me})^+$ (Figure 2). These absorption features indicate the presence of the coordinated phenoxyl radical chromophore also in the dicationic product $(\mathbf{1}^{Me})^{2+}$. The subsequent oxidation of $(\mathbf{1}^{Me})^+$ is presumably localised more at the nickel(II) centre, causing changes in the coordination sphere, which may explain the electrochemically irreversible nature of the second anodic step. However, detailed investigation of this process is beyond the scope of this work. Back reduction of $(\mathbf{1}^{Me})^{2+}$ resulted in the smooth recovery of $(\mathbf{1}^{Me})^+$, thereby excluding any decomposition or irreversible structural change induced by the second anodic reaction.

The X-band EPR spectra of $(\mathbf{1}^{Me})^+$ − generated electrochemically (Figure 3) by bulk electrolysis in CH_2Cl_2 (see Experimental Section) − were recorded in the temperature range 10–240 K. Above the freezing point of CH_2Cl_2 (170–190 K), the EPR spectrum exhibits a single unresolved isotropic signal centred at g_{iso} = 2.04 with a peak-to-peak line width of ca. 100 G. This spectrum resembles those obtained for $[Ni(^{H}L)]^{+}$[7] and $[Ni(^{Cy}L)]^{+}$[6] at T > 190 K. The g_{av} values for the latter spectra (2.03–2.04) are much lower than those expected for a Ni^{III} species (g_{av} values ranging from 2.13 to 2.17),[5] but higher than g factors reported for free[11] or Zn-coordinated[7,10] phenoxyl radicals (2.004–2.005), which are typically close to the free electron value (g_e = 2.0023).[10b] At temperatures below the freezing point of CH_2Cl_2 (10–170 K), the EPR spectrum of $(\mathbf{1}^{Me})^+$ displays a rhombic signal with g_{11} = 2.00, g_{22} = 2.02, g_{33} (broad) = 2.10 and a g_{av} value of 2.04 (obtained from numerical calculation of the average over the whole spectrum). The values g_{11} = 2.00 and g_{22} = 2.02 were obtained directly from the spectrum, and g_{33} was calculated from $g_z = 3g_{av} - g_x - g_y$. Thus, the g_{av} value in frozen CH_2Cl_2 is identical to that obtained above 190 K in fluid solution. This observation is in sharp contrast with the EPR spectra recorded for $[Ni(^{H}L)]^+$ and $[Ni(^{Cy}L)]^+$ at $T < 170$ K, which exhibit an axial signal with $g_\perp > g_\parallel$ and g_{av} of 2.17 and 2.18, respectively.[6,7] The latter spectra are typically observed as a result of a $(d_{z^2})^1$ ground state, which, to the best of our knowledge, can only be achieved for six-coordinate tetragonally elongated nickel(III) compounds,[5] as predicted by the theory.[12]

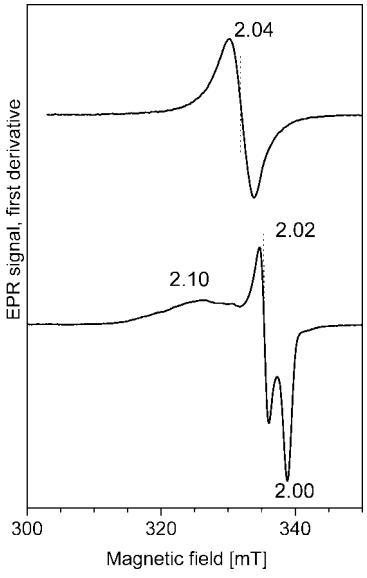

Figure 3. X-band EPR spectrum of electrochemically generated$(\mathbf{1}^{Me})^+$ recorded in frozen CH_2Cl_2 at 30 K (bottom) and at 255 K (top). The numbers indicate the g values (see text).

Thus, the experimental data obtained for $(\mathbf{1}^{Me})^+$ indicate that the electronic structure of the complex remains unchanged in the 10–240 K temperature range. In frozen CH_2Cl_2, the anisotropy becomes resolved. The anisotropy of $(\mathbf{1}^{Me})^+$ and the low g_{av} value are consistent with a Ni^{II} radical complex; the metal centre has a partial Ni^{III} character (vide infra) with a $(dp)^1$ configuration (dp = d_{xy}, d_{xz} or d_{yz}) in a square-planar coordination environment. Such interpretation agrees well with the rhombic or axial EPR

spectra obtained for Ni^{II}–$(N_2O_2)^{\cdot}$ complexes bearing oxamato ($g_{\|} = 2.040 > g_{\perp} = 2.005$;[13] $g_{av} = 2.028$), salicylamidato ($g = 2.09, 2.03, 1.95$; $g_{av} = 2.023$)[7] or semiquinonato ($g_x = 2.0098, 2.0384, 2.1097$; $g_{av} = 2.019$)[14] radical ligands.

DFT calculations were performed with all core states explicitly included, and exchange-correlation effects were treated at the BP86[15a,15b] level of theory. Geometry optimisation, frontier orbitals and EPR parameters were calculated for both parent ($\mathbf{1}^{Me}$) and oxidised compound $(\mathbf{1}^{Me})^+$, and similar treatments were applied for $\mathbf{1}^{H}$ and $(\mathbf{1}^{H})^+$ for comparison. The calculated structural parameters for geometry optimised $\mathbf{1}^{Me}$ and $\mathbf{1}^{H}$ have been found to agree appreciably with the corresponding data obtained by X-ray crystallography: bond lengths are reproduced within ±0.02 Å and bond angles within ±0.2° (Table S1). The calculated *g*-tensor parameters for $(\mathbf{1}^{Me})^+$ are $g_{xx} = 2.1341$, $g_{yy} = 2.0027$, $g_{zz} = 1.9822$. The *z* axis is perpendicular to the plane of the molecule and the *x* axis is the C_2 axis of the system along the plane of the molecule, as indicated in Figure 4. The result is in good agreement (within 0.03) with the experimental data. In particular, the anisotropy in the *g* values has been well reproduced, with the two *g* values close to g_e separated by ca. 0.02 ($g_{yy} - g_{zz}$) and $g_{xx} > g_{yy}$, g_{zz}. We thus tentatively assign the principal *g*-tensor orientations as $g_{11}(2.00) = g_{zz}$, $g_{22}(2.02) = g_{yy}$ and $g_{33}(2.10) = g_{xx}$. This finding supports the validity of the theoretical model and rules out unambiguously a $(d_{z^2})^1$ low-spin Ni^{III} ground state, as had been proposed for $(\mathbf{1}^{H})^+$[7] and $(\mathbf{1}^{Cy})^+$.[6] The calculated singly occupied molecular orbital (SOMO) and the corresponding unpaired spin density distribution of $(\mathbf{1}^{Me})^+$ were also analysed. The SOMO is mainly delocalised on both phenoxy rings, with appreciable contributions of the nickel d_{xz} (6.49%) and d_{yz} (6.33%) orbitals (Figure 4). Consequently, ca. 75% of the unpaired spin is located on the ligand and 25% on the nickel centre. For each phenoxy ring, the typical phenoxy radical pattern with an alternating spin density distribution was obtained; a significant amount of positive spin population at the O (0.115), C_{ortho} (0.08 and 0.06) and C_{para} (0.11) atoms (Figure S2 and Table S2) accounts for ca. 72% of the total spin density. Hence, the calculations agree well with the experimental findings, and $(\mathbf{1}^{Me})^+$ is best described as a nickel(II) complex with a phenoxyl-type radical ligand. In addition, the DFT calculation on $(\mathbf{1}^{H})^+$ shows that the calculated bond parameters of the complex, the nature of the SOMO and the anisotropy in the *g* tensor (calculated *g* values are $g_{zz} = 1.97771$, $g_{yy} = 2.0027$, $g_{xx} = 2.1329$) are essentially identical to the corresponding parameters obtained for $(\mathbf{1}^{Me})^+$. This result is consistent with the calculated absence of spin density on the methyl groups in $(\mathbf{1}^{Me})^+$ and rules out any significant electronic effect of the methyl groups that can explain the EPR discrepancies between $(\mathbf{1}^{Me})^+$ and $(\mathbf{1}^{H})^+$ in frozen CH_2Cl_2. Moreover, in the case of $(\mathbf{1}^{H})^+$, the EPR data in MeOH remain essentially unchanged relative to those obtained in CH_2Cl_2, which suggest a six-coordinate species.[7] Such a coordination environment may have been achieved by either axial coordination of remnant water molecules or intermolecular interactions that may have been prevented by the presence of the methyl groups in the case of $(\mathbf{1}^{Me})^+$.

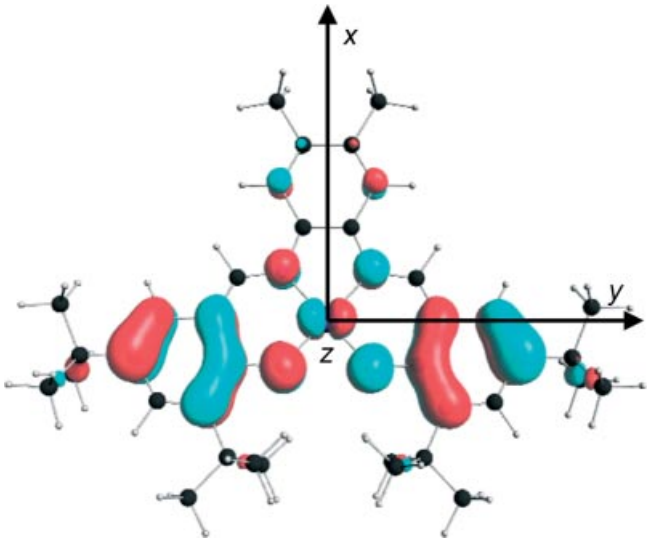

Figure 4. Calculated SOMO for geometry-optimised $(\mathbf{1}^{Me})^+$.

Conclusions

In this communication, we have demonstrated that the one-electron oxidation of the diamagnetic $S = 0$, d^8, low-spin Ni^{II} square-planar compound $[Ni^{II}(^{Me}L)]$ occurs largely on the Schiff-base ligand, yielding $[Ni^{II}(^{Me}L^{\cdot})]^+$. The latter cation is the first example of a thermally stable (within the temperature range 10–295 K) Ni^{II} phenoxyl radical complex. The EPR discrepancies observed (below 170 K) for the reported related complexes $[Ni^{III}(^{H}L)]^+$ and $[Ni^{III}(^{Cy}L)]^+$ cannot be explained by electronic effects. Rather, they may be the result of axial coordination by water (present as impurities) and/or intermolecular interactions, which allow the stabilisation of a six-coordinate Ni^{III} complex. Apparently, this coordination is not stable at higher temperatures and leads to a *g* value in liquid solution that is close to the g_{av} value observed in the present study. Several new bis(salicylidene)diaminenickel(II) complexes with various substituents on the phenylene backbone are being synthesised in order to shed more light on the factors that govern the "spectroscopic" oxidation states of their one-electron oxidation product.

Experimental Section

Synthesis of [Ni(^{Me}L)] ($\mathbf{1}^{Me}$) and Characterisation by NMR Spectroscopy, MS and Elemental Analysis: H_2L (0.568 g, 0.001 mol) in $CHCl_3$ (25 mL) was added to a solution of nickel(II) perchlorate hexahydrate (0.365 g, 0.001 mol) in methanol (10 mL), and the resulting red solution was stirred for 2 h at room temperature. Slow evaporation of the solvent yielded red, needle-shaped crystals within one day, which were isolated, washed with diethyl ether and dried in air. The crystals appeared to be suitable for X-ray structural determination. Yield: 0.46 g (77%). $C_{38}H_{50}N_2NiO_2$ (625.51): calcd. C 72.97, H 8.06, N 4.48; found C 73.04, H 7.71, N 4.40.

ES(+)-MS: m/z = 624.36 [M^+]. IR (neat solid): ν(C=N): 1616 cm^{-1}. UV/Vis (CH_2Cl_2): λ_{max} (ε_{max}, $M^{-1}cm^{-1}$) = 268 (42 400), 299 (18 300), 312 (sh.), 385 (29 800), 475 (sh.), 499 (8 900) nm. ^1H NMR (300 MHz, $CDCl_3$): δ = 8.14 (s, 2 H, H–C=N), 7.44 (s, 2 H, H_{PhN_2}), 7.39 (d, ^4J = 2.7 Hz, 2 H, H_{PhO}), 7.09 (d, ^4J = 2.7 Hz, 2 H, H_{PhO}), 2.30 (s, 6 H, CH_3), 1.46 [s, 18 H, $C(CH_3)_3$], 1.30 [s, 18 H, $C(CH_3)_3$] ppm. All measurements were performed on locally available standard instruments.

Electrochemistry: Each experiment was performed under dinitrogen using dry, distilled and degassed CH_2Cl_2. The cyclic voltammogram of the studied compound $\mathbf{1}^{Me}$ (10^{-3} M) in CH_2Cl_2 containing [NBu^n_4][ClO_4] (4×10^{-1} M) as the background electrolyte was recorded at room temperature with a glassy carbon working electrode, a Pt plate auxiliary electrode and a Ag/AgCl reference electrode. The electrode potentials are referenced against the Fc/Fc^+ couple that was used as the internal standard. The oxidised species $(\mathbf{1}^{Me})^+$ was generated by controlled potential electrolysis (CPE) performed on $\mathbf{1}^{Me}$ (10^{-3} M) at 263 K in a CH_2Cl_2 solution containing [NBu^n_4][ClO_4] (4×10^{-1} M) as the background electrolyte. The electrolytic cell consisted of a Pt gauze basket working electrode, a Pt gauze auxiliary electrode and a Ag/AgCl reference electrode. Both CV and CPE measurements were performed by using an Autolab PGSTAT20 potentiostat.

UV/Vis Spectroelectrochemistry: UV/Vis spectroelectrochemical experiments at low temperatures were performed with a cryostatted optically transparent thin-layer electrochemical (OTTLE) cell equipped with CaF_2 windows and a Pt minigrid working electrode (32 wires per cm).[16a] The electrolysis at room temperature was conducted with another home-made demountable OTTLE cell.[16b] The concentrations of the solutions were typically 3×10^{-1} M in the supporting electrolyte ([NBu^n_4][ClO_4]) and 10^{-3} M in the analyte. The working electrode potential of the spectroelectrochemical cells was controlled with a PA4 potentiostat (EKOM, Polná, Czech Republic). A thin-layer cyclic voltammogram was recorded during the course of each spectroelectrochemical experiment. The electronic absorption spectra were obtained with a HP 8453 diode array spectrophotometer.

EPR Spectroscopy: X-band (9.48 GHz) cw-EPR spectra were recorded by using a ELEXSYS E680 (Bruker, BioSpin, Rheinstetten) spectrometer with a TE102 resonator. Sample solutions of electrochemically generated $(\mathbf{1}^{Me})^+$ (vide ultra) were rapidly transferred under exclusion of dioxygen into an X-band quartz tube (4-mm inner diameter), which was immediately frozen and stored in liquid nitrogen. The measurements were performed at temperatures from 10 to 240 K using an Oxford ESR 900H cryostat. The microwave power supplied to the resonator was varied in the range 0.2–2 mW; a 100-kHz magnetic field modulation with a peak-to-peak amplitude of 0.5 mT was used.

DFT Calculations: The calculations were performed with the Amsterdam Density Functional (ADF 2005) program system.[15c,15d] A Slater-type orbital basis set of triple zeta quality for the valence orbitals was used, augmented with a polarization function, cf. the standard TZP basis.[15e] Calculations were performed on isolated molecules, without inclusion of solvent molecules.[15f]

X-ray Crystallographic Study of $\mathbf{1}^{Me}$: Crystal data: $C_{38}H_{50}N_2NiO_2$, red, needle, F_w = 625.51, triclinic, space group $P\bar{1}$, a = 9.2500(10) Å, b = 14.865(2) Å, c = 14.951(2) Å, α = 119.220(10)°, β = 101.650(10)°, γ = 92.310(10)°, V = 1733.9(4) $Å^3$, d = 1.198 $g\,cm^{-3}$, Z = 2, T = 173(2) K, $F(000)$ = 627, μ(Mo-K_α) = 0.593 mm^{-1}. A transparent, red, needlelike single crystal of $0.25\times0.05\times0.05$ mm was mounted on a Lindemann glass capillary and transferred into the cold nitrogen stream of a Nonius KappaCCD diffractometer on a rotating anode (Mo-K_α radiation, graphite monochromator, λ = 0.71073 Å). 27617 independent reflections (7944 unique; R_{int} = 0.117) were collected. The intensity data were corrected for Lorentz and polarisation effects and for absorption. The structure was solved by direct methods. The programs COLLECT[17a] SHELXS-97[17b] and SHELXL-97[17c] were used for data reduction, structure solution and structure refinement, respectively. The final agreement factors are R_1 = 0.0657 for 4241 data with $F > 4\sigma(F)$ and R_1 = 0.1554, wR_2 = 0.1433 for 7944 data. All non-hydrogen atoms were refined anisotropically. Hydrogen atoms were placed at idealised positions and allowed to ride on the connecting atom. CCDC-622859 contains the supplementary crystallographic data for this paper. These data can be obtained free of charge from The Cambridge Crystallographic Data Centre via www.ccdc.cam.ac.uk/data_request/cif.

Supporting Information (see footnote on the first page of this article): Cyclic voltammogram of $\mathbf{1}^{Me}$, in CH_2Cl_2, containing [NBu^n_4][ClO_4] (0.4 M), plot of the distribution of the non-zero spin populations, calculated bond lengths [Å] and angles [°] for the optimised structure of $\mathbf{1}^{Me}$ and $\mathbf{1}^{H}$, list of individual atomic electron spin density calculated for $(\mathbf{1}^{Me})^+$.

Acknowledgments

This work has been supported financially by the Graduate Research School Combination "Catalysis", a joint activity of the graduate research schools NIOK, HRSMC and PTN. Financial support from COST Action D21/003/01 and the Netherlands Technology Research Foundation (STW) applied science division of the Netherlands Organisation for Scientific Research (NWO) are thankfully acknowledged (grant number 5751).

[1] Recent reviews: a) P. Chaudhuri, K. Wieghardt, *Prog. Inorg. Chem.* **2001**, *50*, 151–216; b) C. G. Pierpont, *Coord. Chem. Rev.* **2001**, *216–217*, 99–125; c) C. G. Pierpont, *Coord. Chem. Rev.* **2001**, *219–221*, 415–433; d) W. Kaim, *Dalton Trans.* **2003**, 761–768.

[2] Recent reviews: a) J. Stubbe, W. A. van der Donk, *Chem. Rev.* **1998**, *98*, 705–762; b) J. Stubbe, D. G. Nocera, C. S. Yee, M. C. Y. Chang, *Chem. Rev.* **2003**, *103*, 2167–2201.

[3] J. W. Whittaker, *Chem. Rev.* **2003**, *103*, 2347–2363.

[4] a) P. Gütlich, A. Dei, *Angew. Chem. Int. Ed. Engl.* **1997**, *36*, 2734–2736; b) P. Gütlich, Y. Garcia, T. Woike, *Coord. Chem. Rev.* **2001**, *219–221*, 839–879; c) D. A. Shultz, in *Magnetoscience – From Molecules to Materials* (Eds.: S. Miller, M. Drillon), Wiley-VCH, New York, **2001**.

[5] a) R. S. Drago, E. I. Baucom, *Inorg. Chem.* **1972**, *11*, 2064–2069; b) N. Takvoryan, K. Farmery, V. Katovic, F. V. Lovecchio, E. S. Gore, L. A. Anderson, F. V. Lovecchio, E. S. Gore, D. H. Busch, *J. Am. Chem. Soc.* **1974**, *96*, 731–742; c) D. H. Busch, *J. Am. Chem. Soc.* **1974**, *96*, 3109–3118; d) A. Bencini, L. Fabbrizzi, A. Poggi, *Inorg. Chem.* **1981**, *20*, 2544–2549; e) S. A. Jacobs, D. W. Margerum, *Inorg. Chem.* **1984**, *23*, 1195–1201; f) H. J. Krüger, R. H. Holm, *Inorg. Chem.* **1987**, *26*, 3645–3647; g) P. A. Connick, K. A. Macor, *Inorg. Chem.* **1991**, *30*, 4654–4663; h) T. J. Collins, T. R. Nichols, E. S. Uffelman, *J. Am. Chem. Soc.* **1991**, *113*, 4708–4709; i) F. Azevedo, M. A. Carrondo, B. Castro, M. Convery, D. Domingues, C. Freire, M. T. Duarte, K. Nielsen, I. C. Santos, *Inorg. Chim. Acta* **1994**, *219*, 43–54; j) D. Pinho, P. Gomes, C. Freire, B. De Castro, *Eur. J. Inorg. Chem.* **2001**, 1483–1493; k) B. De Castro, C. Freire, *Inorg. Chem.* **1990**, *29*, 5113–5119; l) C. Freire, B. De Castro, *J. Chem. Soc., Dalton Trans.* **1998**, 1491–1498; m) I. C. Santos, M. Vilas-Boas, M. F. M. Piedade, C. Freire, M. T. Duarte, B. De Castro, *Polyhedron* **2000**, *19*, 655–664; n) M. A. Carrondo,

B. De Castro, A. M. Coelho, D. Domingues, C. Freire, J. Morais, *Inorg. Chim. Acta* **1993**, *205*, 157–166; o) K. Nag, A. Chakravorty, *Coord. Chem. Rev.* **1980**, *33*, 87–147; p) Z. Xiao, B. O. Patrick, D. Dolphin, *Inorg. Chem.* **2003**, *42*, 8125–8127; q) P. J. Alonso, L. R. Falvello, J. Fornies, A. Martin, B. Menjon, G. Rodriguez, *Chem. Commun.* **1997**, 503–504; r) H.-J. Krüger, G. Peng, R. H. Holm, *Inorg. Chem.* **1991**, *30*, 734–742.

[6] Y. Shimazaki, F. Tani, K. Fukui, Y. Naruta, O. Yamauchi, *J. Am. Chem. Soc.* **2003**, *125*, 10512–10513.

[7] O. Rotthaus, O. Jarjayes, F. Thomas, C. Philouze, C. Perez Del Valle, E. Saint-Aman, J.-L. Pierre, *Chem. Eur. J.* **2006**, *12*, 2293–2302.

[8] R. Kannappan, S. Tanase, D. M. Tooke, A. L. Spek, I. Mutikainen, U. Turpeinen, J. Reedijk, *Polyhedron* **2004**, *23*, 2285–2291.

[9] E. R. Altwicker, *Chem. Rev.* **1967**, *67*, 475–531.

[10] a) L. Benisvy, E. Bill, A. J. Blake, D. Collison, E. S. Davies, C. D. Garner, G. McArdle, E. J. L. McInnes, J. McMaster, S. Ross, C. Wilson, *Dalton Trans.* **2006**, 258–267; b) It should be noted that an apparent typical "Ni^{III}" g_{av} value of 2.13 has been obtained for an octahedral Ni^{II} phenoxyl radical complex; the reported spectrum was in sharp contrast to that of a Ni^{III} species and covered the 100–400 mT region and was assigned to an $S = 3/2$ ground state originating from strong intramolecular ferromagnetic coupling between the Ni^{II} $S = 1$ and the radical $S = 1/2$ centres. See J. Müller, A. Kikuchi, E. Bill, T. Weyhermüller, P. Hildebrandt, L. Ould-Moussa, K. Wieghardt, *Inorg. Chim. Acta* **2000**, *297*, 265–277.

[11] a) T. Maki, Y. Araki, Y. Ishida, O. Onomura, Y. Matsumura, *J. Am. Chem. Soc.* **2001**, *123*, 3371–3372; b) F. Thomas, O. Jarjayes, H. Jamet, S. Hamman, E. Saint-Aman, C. Duboc, J.-L. Pierre, *Angew. Chem. Int. Ed.* **2004**, *43*, 594–597; c) L. Benisvy, R. Bittl, E. Bothe, C. D. Garner, J. McMaster, S. Ross, C. Teutloff, F. Neese, *Angew. Chem. Int. Ed.* **2005**, *44*, 5314–5317.

[12] A. H. Maki, N. Edelstein, A. Davidson, R. H. Holm, *J. Am. Chem. Soc.* **1964**, *86*, 4580–4587.

[13] X. Ottenwaelder, R. Ruiz-García, G. Blondin, R. Carasco, J. Cano, D. Lexa, Y. Journaux, A. Aukauloo, *Chem. Commun.* **2004**, 504–505.

[14] K. S. Min, T. Weyhermüller, E. Bothe, K. Wieghardt, *Inorg. Chem.* **2004**, *43*, 2922–2931.

[15] a) A. D. Becke, *Phys. Rev. A* **1988**, *38*, 3098–3100; b) J. P. Perdew, *Phys. Rev. B* **1986**, *33*, 8822–8824; c) E. J. Baerends, D. E. Ellis, P. Ros, *Chem. Phys.* **1973**, *2*, 41–51; d) C. Fonseca Guerra, J. G. Snijders, G. te Velde, E. J. Baerends, *Theor. Chem. Acc.* **1998**, *99*, 391–403; e) Scientific Computing and Modeling (SCM), Theoretical Chemistry, Vrije Universiteit Amsterdam, URL: http://www.scm.com; f) For details on the procedure for computing EPR parameters and ADF implementations, the reader is referred to the online documentation of ADF.[15e]

[16] a) F. Hartl, R. P. Groenestein, T. Mahabiersing, *Collect. Czech. Chem. Commun.* **2001**, *66*, 52–66; b) M. Krejčík, M. Daněk, F. Hartl, *J. Electroanal. Chem.* **1991**, *317*, 179–187.

[17] a) B. V. Nonius, *COLLECT*, Software Suite, Delft University, Delft, **2004**; b) G. M. Sheldrick, *SHELXS-97, Program for Crystal Structure Determination*, University of Göttingen, Germany, **1997**; c) G. M. Sheldrick, *SHELXL-97, Program for Crystal Structure Refinement*, University of Göttingen, Germany, **1997**.

Received: October 27, 2006
Published Online: January 8, 2007

